Catalysis Today 175 (2011) 2–11

Contents lists available at ScienceDirect

Catalysis Today

journal homepage: www.elsevier.com/locate/cattod

Reactivity of NH_3 over (Fe)/H-ZSM-5 zeolite: Studies of temperature-programmed and steady-state reactions

Xiaoyin Chen[a], Wei Li[b], Johannes W. Schwank[a,*]

[a] Department of Chemical Engineering, University of Michigan, Ann Arbor, MI 48109, USA
[b] General Motors Global Research and Development, Warren, MI 48090, USA

ARTICLE INFO

Article history:
Received 29 October 2010
Received in revised form 6 May 2011
Accepted 16 May 2011
Available online 17 June 2011

Keywords:
Ammonia
Selective catalytic reduction
NO
NO_2
ZSM-5
Acidity
Iron oxide
Adsorption
Release
Temperature programmed surface interaction (TPSI)

ABSTRACT

The NH_3 reactivity was investigated over H-ZSM-5 and iron oxide deposited H-ZSM-5 by temperature-programmed surface interaction (TPSI) of adsorbed NH_3 (NH_3(ad)) with NO, O_2, and "NO + O_2", and by steady-state dynamic reactions consisting of "NH_3 + NO", "NH_3 + O_2", and "NH_3 + NO + O_2" systems. It was found that O_2 primarily interacts with NH_3(ad) on Brønsted acid sites. NO mainly interacts with NH_3(ad) on Lewis acid sites, whereas its interaction with NH_3(ad) on Brønsted acid sites results in N_2O formation. TPSI provides direct evidence of the "fast" reaction of NO/NO_2 with NH_3(ad) on Brønsted acid sites in "NO + O_2" environment, where O_2 concentration plays a critical role. Iron oxide enhances all interactions, particularly those with NH_3(ad) on Brønsted acid sites, as witnessed by both TPSI and steady-state reactions. But, iron oxide does not change the activation energy barrier for NH_3 conversion, indicating that both acid sites and iron oxide are essential for NH_3 SCR of NO_x. As a result, a dual mechanism over Lewis and Brønsted acid sites was proposed.

1. Introduction

As effective solutions to catalytically eliminate NO_x in automobile aftertreatment systems, lean NO_x trap (LNT) and selective catalytic reduction (SCR) catalysts have received attention [1]. When operating a BaO–Pt/Al_2O_3 LNT model catalyst during the rich cycle, NH_3 was found to be the primary NO_x reduction product. A zeolite catalyst placed downstream of the LNT can capture this rich-cycle generated NH_3, and during the lean cycle the adsorbed NH_3 can be used to reduce NO_x via NH_3-SCR [2,3]. The combination of LNT with SCR opens a promising window for effectively treating lean NO_x emitted from diesel engines [4–6].

Fe-based zeolites, in particular Fe-exchanged ZSM-5, have been recognized as highly efficient catalysts for NH_3 SCR of NO [7–10]. So far, extensive studies have been done on the nature of active Fe species. However, there are debates in the literature about the role of non-framework iron species in Fe-exchanged zeolites, as iron oxide (Fe_2O_3 and Fe–O oligomers) and exchanged cationic iron species could co-exist [7,11–13]. The exchanged iron species, including Fe^{2+}, Fe^{3+} or oxo-Fe^{3+} cations were considered to be active sites [9,10,12–15]. Some studies found that iron oxide in zeolites was not active for the SCR reaction [14,16]. However, others reported that supported Fe_2O_3 [17–21] and dispersed iron oxide in ZSM-5 [22–24] and in Beta [25,26] were highly active for NH_3 SCR of NO. In fact, iron oxide as catalytic component in Fe-BEA catalysts with comparably high activity can be reproducibly prepared by simple incipient wetness impregnation with $Fe(NO_3)_3$ [24–26] and can be used for industrial scale applications. When SCR of NO_x was investigated with methane and butane as reducing agents over (In,Fe)-zeolites, a significant increase of NO_x to N_2 conversion was observed, likely due to Fe_2O_3 improving the NO to NO_2 reaction rate [27].

Surface acidity is one of the most important characteristics of a zeolite catalyst. The effect of acidity on NH_3 SCR of NO has been extensively investigated, but no clear conclusion has been reached in the literature [13,28,29]. Although the number of Brønsted acid sites decreases with the increase of exchange degree of cationic species, it is generally accepted that when SCR proceeds over cation-exchanged zeolites, Brønsted acid sites are required for the activation of ammonia and reduction of NO_x to N_2 [7,15,30,31], and an acid-catalyzed step may be rate-determining especially at

* Corresponding author. Tel.: +1 734 764 3374; fax: +1 734 763 0459.
E-mail addresses: xychen@umich.edu (X. Chen), wei.1.li@gm.com (W. Li), schwank@umich.edu (J.W. Schwank).

0920-5861/$ – see front matter © 2011 Elsevier B.V. All rights reserved.
doi:10.1016/j.cattod.2011.05.010

low temperatures [29]. Long and Yang concluded that the NH_3 SCR needs two types of active sites: Brønsted acid sites for NH_3 adsorption and Fe^{3+} ions for NO oxidation to NO_2 [32]. However, a comparative study from Liu et al. for iron oxide supported on BEA, TiO_2, and Al_2O_3 showed no evidence that the presence of either Brønsted or Lewis acidity is key to the activation of ammonia [24]. The results from Peña et al. showed Brønsted acid sites are not necessary, while Lewis acid sites are required for TiO_2-supported iron oxide [33]. For Fe-ZSM-5 catalyst, Brandenberger et al. revealed that Brønsted acidity may not be required for adsorbing or activating ammonia [13], but acid sites are still necessary to disperse and bind cationic Fe species in zeolites [13,34].

Recently, fast SCR has received much attention. When NO_2 is present in the emissions, both NO and NO_2 are consumed in an 1:1 ratio according to the reaction:

$$2NH_3 + NO + NO_2 \rightarrow 2N_2 + 3H_2O \quad (1)$$

This phenomenon was first observed on Fe_2O_3/TiO_2 catalyst [35] and later was also found over Fe-based zeolites [7,13,15,36–40]. The uniqueness is that NO first has to be oxidized to NO_2 [13,32,36,41], which is believed to be the rate-determining step of the SCR mechanism [16,38,39,42,26,43]. However, the effect of acidity and the role of iron oxide in zeolites on fast SCR [41] are still poorly understood.

NH_3 is a base that has been widely used as a probe molecule to characterize the surface acidity of zeolites [44,45]. NH_3 is also a reductant for the SCR of NO. As the activation of NH_3 is a critical step for NH_3 SCR of NO [13,24,38], the objective of the present work is to focus on NH_3 reactivity in order to better understand NH_3 SCR. Therefore, comparative studies of temperature-programmed surface interaction (TPSI) via the release of adsorbed NH_3 in different reactive environments (NO, O_2, and "NO + O_2") and the steady-state dynamic reactions of NH_3 over H-ZSM-5 (H-Z) and iron oxide modified H-ZSM-5 (Fe/H-ZSM-5) are presented in this work to elucidate the acid effect on NH_3 activation and conversion.

2. Experimental

2.1. Materials and characterization

H-ZSM-5 was obtained via calcination of NH_4-ZSM-5 (Si/Al = 11.5, Zeolyst) at 550 °C in air or via in situ transformation in N_2 flow prior to NH_3 adsorption. Fe/H-ZSM-5 was prepared by incipient wetness impregnation of NH_4-ZSM-5 with $Fe(NO_3)_3$. Following the impregnation at room temperature with $Fe(NO_3)_3$ aqueous solution, samples were dried at 110 °C and then calcined at 550 °C in air for 2 h with a fast heating rate (80 °C/min) to allow $Fe(NO_3)_3$ decomposition to iron oxide during NH_4-ZSM-5 transformation into H-ZSM-5. The aim of the incipient wetness impregnation of $Fe(NO_3)_3$ combined with the fast heating procedure was to deposit iron oxide into the zeolite, whereas a proton exchange was not explicitly intended. In fact, with a heating rate of 10 °C/min in air flow, complete decomposition of $Fe(NO_3)_3$ into iron oxide occurred as proven by TGA (weight loss)-IR (N_2O evolution). The iron oxide deposited H-ZSM-5 sample was denoted as FeZ. BET surface area and pore properties of samples calcined at 550 °C were analyzed by N_2 physisorption at −196 °C on an ASAP 2020 instrument (Micromeritics). Powder X-ray diffraction (XRD) was carried out on a rotating anode Rigaku RU-200B series X-ray diffractometer.

2.2. NH_3 adsorption and release

NH_3 adsorption and subsequent in situ release were performed with a total gas flow of 100 ml/min on a thermogravimetric analyzer (TA Q500) combined with an on-line FT-IR spectrometer (Nicolet 380) for analysis of evolved gases. After the sample (25–35 mg) was heated (10 °C/min) to 550 °C and held in a N_2 flow for 60 min, the system was cooled to 100 °C for NH_3 adsorption for 60 min in a 1% NH_3/N_2 flow. Prior to NH_3 release, the system was purged with a pure N_2 flow for another 60 min to remove weakly and physically adsorbed NH_3. The release of adsorbed NH_3 (NH_3(ad)) was then carried out with a heating ramp of 10 °C/min in N_2, NO, and O_2 environment, respectively. It should be pointed out that the release of NH_3(ad) in N_2 environment represents a typical NH_3 TPD experiment. The release of NH_3(ad) was also performed in "NO + O_2" environment. In this case, NO and O_2 were not premixed, but fed into the TGA reactor separately with O_2/N_2 fed through the balance-side flow while NO/N_2 was fed through the sample-side gas flow. Unless specifically noted, the concentrations of O_2 and NO in O_2 and NO environments were 12.6% and 2000 ppm while the concentrations of O_2 and NO in "NO + O_2" environment were 16.8% and 2000 ppm, respectively. It should be emphasized that pure NH_3 desorption can only be accomplished in N_2 environment. In reactive gas environments, the release is best described as a removal process of NH_3(ad), as both desorption and TPSI may occur in NO, O_2, and "NO + O_2" environments.

2.3. Steady-state reaction

Steady-state reaction for NH_3 conversion by the reactions of "NH_3 + NO", "NH_3 + O_2", and "NH_3 + O_2 + NO" were carried out using a packed-bed reactor. A quartz tube reactor with approximately 4.5 mm inner diameter was used and loaded with 100 mg catalyst (40–60 mesh size). For all steady-state reactions ("NH_3 + NO", "NH_3 + O_2", and "NH_3 + NO + O_2"), the reactor inlet gas flow was composed of 500 ppm NH_3, 500 ppm NO, and/or 4 vol.% O_2, and controlled by mass flow controllers. The gas flow was balanced by He to reach a total gas flow rate of 450 ml/min (STP), corresponding to GHSV of ~140,000 h^{-1}. The analysis of gas components in the inlet and outlet of the reactor was performed by a gas chromatograph (Varian) for N_2 and by an IR spectrometer (Nicolet 380) for NH_3, NO, N_2O, and NO_2.

3. Results and discussion

3.1. Basic properties of H-ZSM-5 and Fe/H-ZSM-5

H-ZSM-5 provides both Brønsted (B) and Lewis (L) acid sites for NH_3 adsorption. NH_3 adsorption associates with H^+ on B acid sites to form ammonium (NH_4^+), while NH_3 adsorbs on L acid sites by donating lone-pair electrons. The acidic sites are essitial for NH_3 adsorption in ZSM-5. The NH_3 adsorption capacity (NAC), which can be measured by the amount of NH_3(ad) released in N_2 environment, reflects the number of acid sites and relies on the ratio of incorporated aluminium to silicon in the ZSM-5 framework. Table 1 shows the properties of H-ZSM-5 and Fe/H-ZSM-5. Iron oxide deposited zeolites prepared by the simple incipient wetness impregnation of $Fe(NO_3)_3$ were reported in previous studies [24,25,46]. In our work the formation of iron oxide was confirmed by the decomposition of $Fe(NO_3)_3$ using TGA (weight loss)-IR (N_2O evolution) characterization (heating rate of 10 °C/min), which was performed prior to NH_3 adsorption (see thereafter). The NAC of Fe/H-ZSM-5 was not changed much, indicating that no proton exchange occurred. A slight (3%) decrease in NAC (1.43) was observed in sample FeZ-1, confirming no significant impact of iron oxide deposition on acidity of H-ZSM-5. The observed slight NAC decrease is attributable to the partial coverage of acidic sites by iron oxide that leads to the physical blockage of the NH_3 adsorption. With the increase of iron oxide loading to 6.62 wt.%, a 30% decrease of NAC (1.04) was observed, attributable to the blockage of acidic sites (Al and H^+ sites) by the coverage of iron oxide and likely also to the partial dealumination

Table 1
Sample properties.

Sample	Fe_2O_3 loading (wt.%)	NAC[a] (NH_3/Al, atomic)	Surface area (m^2/g)		Micropore volume[b] (cm^3/g)
			BET	Micro[b]	
H-ZSM-5	0	1.48	348	252	0.133
FeZ-1	3.43	1.43	338	249	0.132
FeZ-2	6.62	1.04	323	230	0.122

[a] NH_3 adsorption capacity.
[b] Pore size less than 1.0 nm.

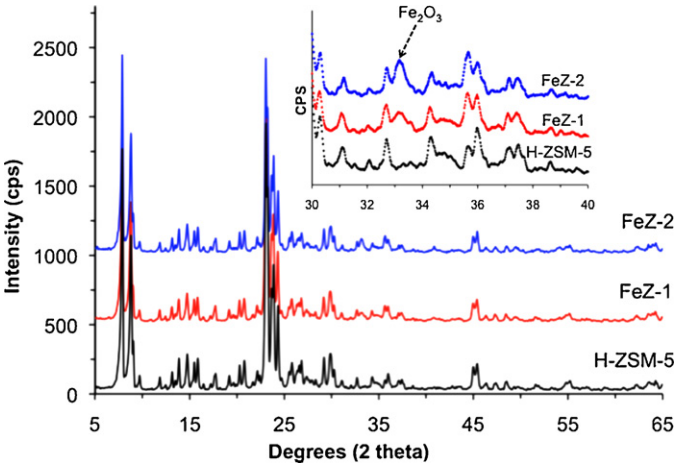

Fig. 1. XRD patterns of H-ZSM-5, FeZ-1, and FeZ-2.

of ZSM-5 during calcination at 550 °C in air. Obvious dealumination was observed in ^{27}Al NMR spectra (not shown here) of post calcined NH_4-ZSM-5 at 550 °C in air.

The deposition of iron oxide in H-ZSM-5 can also be confirmed by the decrease of BET surface area of H-ZSM-5. If a mechanical mixing of H-ZSM-5 with equivalent Fe_2O_3 loading was assumed, the BET surface area of samples FeZ-1 and FeZ-2 decreased by 2.8% and 7.2%, respectively, closely consistent with the Fe_2O_3 loading (3.43 wt.% and 6.62 wt.%). Comparison of the micropore surface area and pore volume of the iron containing samples with H-ZSM-5 shows that the deposition of iron oxide led to the decrease of micropore features due to pore clogging. XRD showed (Fig. 1) a very weak extra diffraction peak that did not belong to ZSM-5. This peak is assignable to the (1 0 4) plane of Fe_2O_3 phase (PDF#00-033-0664) and its intensity was increased with increased Fe loading. Furthermore, the FeZ samples after aging at 750 °C in 10% steam gave clear XRD peaks characteristic for Fe_2O_3. These XRD results indicate that in the calcined samples iron oxide is highly dispersed.

3.2. Release of NH_3(ad) over H-ZSM-5

The best method to characterize whether Fe species are exchanged with protons is the direct measurement of NH_3 adsorption. As a result, release of NH_3(ad) over H-ZSM-5 in N_2 environment, i.e., NH_3 TPD, was investigated by TGA-IR. The thermogravimetric (TG) and derivative thermogravimetric (DTG) curves and the integration of the IR band of released NH_3 on-line evolved from TGA operation provide quantitative results for the NH_3 adsorption features. Two release peaks in both DTG and IR curves were observed (Fig. 2). The peaks at low temperature and at high temperature reflect the desorptions of NH_3(ad) on L and B acid sites, respectively [47]. From the amount of released NH_3 measured by both TGA as well as the integration of the NH_3 IR band, the number of acid sites on the sample can be estimated.

The release of NH_3(ad) in the reactive gas environments (O_2, NO, and "NO + O_2") is also shown in Fig. 2. In these cases, the DTG curves reflect the removal of total NH_3(ad) from the zeolite via either NH_3 desorption or interaction with reactive gas, while IR identifies N-containing oxide gases evolved from TGA including NH_3 and products (N_2O, NO, and NO_2) formed by reactive gas. As compared with desorption in N_2 flow, the peak temperatures in the DTG curves of NH_3 released in O_2 environment did not change (Fig. 2A), while the high-temperature (HT) NH_3 IR peak shifted from 415 °C to 400 °C (Fig. 2B). When the release was conducted in an NO environment, the low-temperature (LT) peak in the DTG curves shifted from 198 °C to 135 °C, while both LT and HT IR peaks were significantly reduced in intensity. This indicates the strong interaction of NO with NH_3(ad) on both L and B acid sites at temperatures lower than required for NH_3 desorption. Fig. 3A shows the product distribution during NH_3(ad) release in NO environment. A strong N_2O peak was observed at the same peak temperature (394 °C) of the desorption of NH_3(ad) on B acid sites. This provides evidence that N_2O is one of the products of NO interacting with NH_3(ad) on B acid sites. It is unlikely that N_2O, if it were the product from the interaction on L acid sites, would not be released at the lower temperature of about 200 °C. The co-feeding of NO and O_2 (i.e., "NO + O_2" environment) accelerated the interaction of NH_3(ad) on both types of acid sites. In the DTG curves (Fig. 2A), the LT peak shifted from 198 °C in N_2 to 135 °C in "NO + O_2", while the HT peak shifted by more than 100 °C from 399 °C to 282 °C. In addition, the ending temperature of the weight loss curve, corresponding to the complete removal of NH_3(ad), significantly decreased to *ca* 310 °C from *ca* 580 °C in N_2. In the NH_3 IR curves (Fig. 3B), no NH_3 desorption peak from B acid sites was observed, only a very small peak at 200 °C corresponding to the NH_3 desorption from L acid sites appeared. No obvious N_2O formation peak was observed. The presence of O_2 also accelerated the interaction of adsorbed NH_3 with NO_x. Two negative peaks at 286 °C were observed, as shown in Fig. 3B, which were indicative of simultaneous consumption of NO and NO_2 due to the interactions with adsorbed NH_3. As the position of the negative NO and NO_2 peaks (286 °C) is much higher than the release peak (200 °C) of NH_3(ad) on L acid sites, the simultaneous consumption of NO and NO_2 should be attributable to the interaction of "NO + NO_2" with NH_3(ad) on B acid sites. It should be noted that the integration intensities of NO and NO_2 IR signals depend on the IR absorption efficiency. If a comparison were made for the relative concentrations of NO and NO_2, the integrated IR intensity of NO_2 should be divided by 13.6 as IR absorption of NO_2 is 13.6 times more sensitive than NO [48].

Quantitative comparisons of the amount of released NH_3 can be made by integration of the NH_3 IR band. The results are presented in Table 2 in form of a percentage ratio of the integrated intensity of the NH_3 IR band for released NH_3 in reactive gas to that (NAC) in the pure N_2 flow. Table 2 shows that the released NH_3 amount in O_2 was 76% of that released in N_2, indicating that 24% of adsorbed NH_3 participated in the interaction with O_2 during the heating ramp. Less NH_3 was released from B acid sites (71%) than from L acid sites (82%), indicating that more NH_3(ad) on B acid sites interacted with O_2. It is also seen from Table 2 that NO is

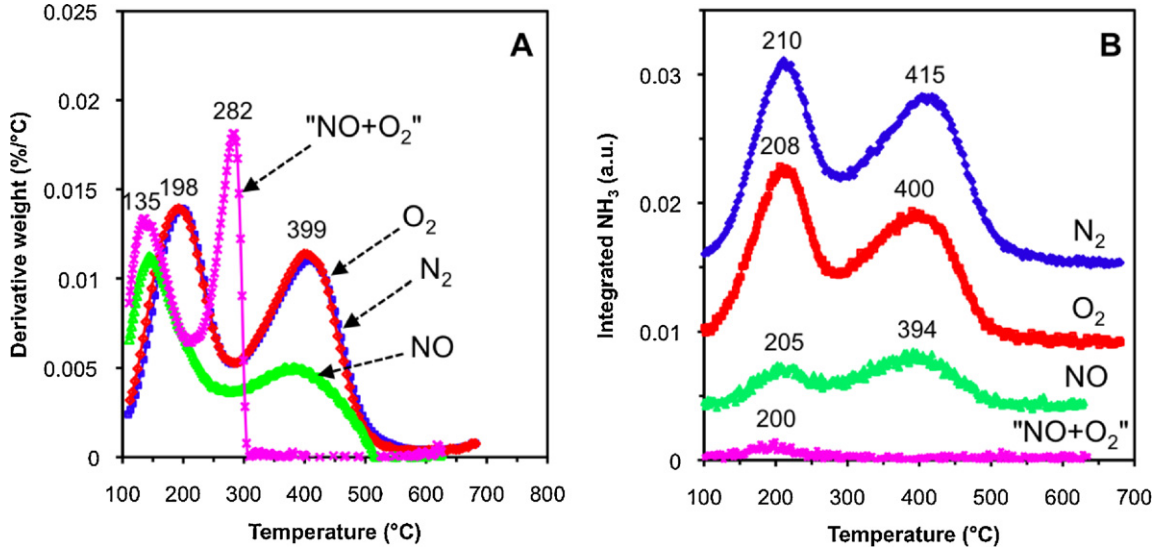

Fig. 2. DTG curves (A) and integrated NH_3 IR (B) during temperature-programmed release of NH_3(ad) on H-ZSM-5 in different environments.

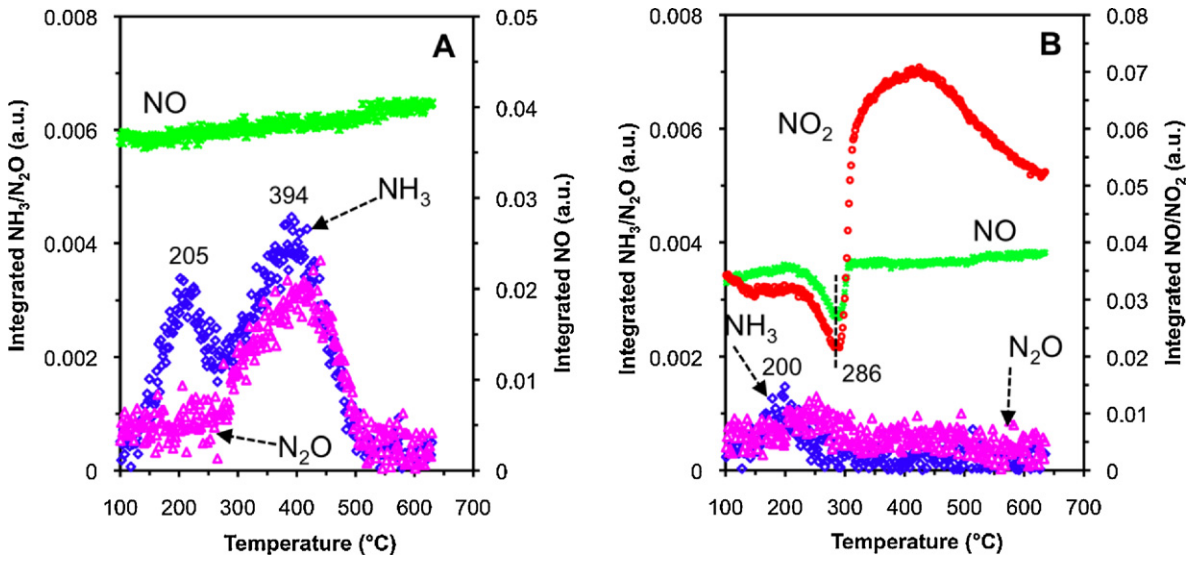

Fig. 3. Distribution of NH_3, N_2O, NO, and NO_2 during temperature-programmed release of NH_3(ad) on H-ZSM-5 in NO (A) and "NO + O_2" (B) environments.

more reactive than O_2 to interact with adsorbed NH_3, as only 67% of pre-adsorbed NH_3 was released in 2000 ppm of NO environment. Further, NO more readily interacted with NH_3(ad) on L acid sites than with NH_3(ad) on B acid sites, as less NH_3 was released from L acid sites than from B acid sites. For NH_3 release in "NO + O_2", it is seen that "NO + O_2" is more reactive than either NO or O_2, as only 6% of adsorbed NH_3 was released. The other 94% of adsorbed NH_3 was removed by interaction, not by desorption. More specifically, interaction with "NO + O_2" removed 98% of NH_3(ad) on B acid sites and 90% of NH_3(ad) on L acid sites. The presence of O_2 significantly promotes the interaction as evidenced by the simultaneous consumption of NO and NO_2 (Fig. 3B). The removal peak temperature (286 °C) in "NO + O_2" was 108 °C lower than for the desorption (394 °C) in NO only.

NH_3 adsorption in H-ZSM-5 is based on the acid–base interaction. The subsquent desorption at elevated temperatures depends on the strength of such acid–base interactions. If the desorption is performed in a reactive gas environment, a portion of adsorbed NH_3 would be removed by interaction, instead of by the desorption from acid sites. TPSI experiments showed that NO prefers to inter-

Table 2
Released NH_3 amount over H-ZSM-5 in different environments.

Released NH_3	In N_2[a]	In O_2[a]	In NO		In NO + O_2[b]
			a	b	
Total (%)	100	76	67	45	6
L acid site (%)	100	82	46	30	10
B acid site (%)	100	71	85	61	2

H-ZSM-5 was obtained from NH_4-ZSM-5 by in situ transformation in N_2 flow[a] or by calcination at 550 °C in air atmosphere[b].

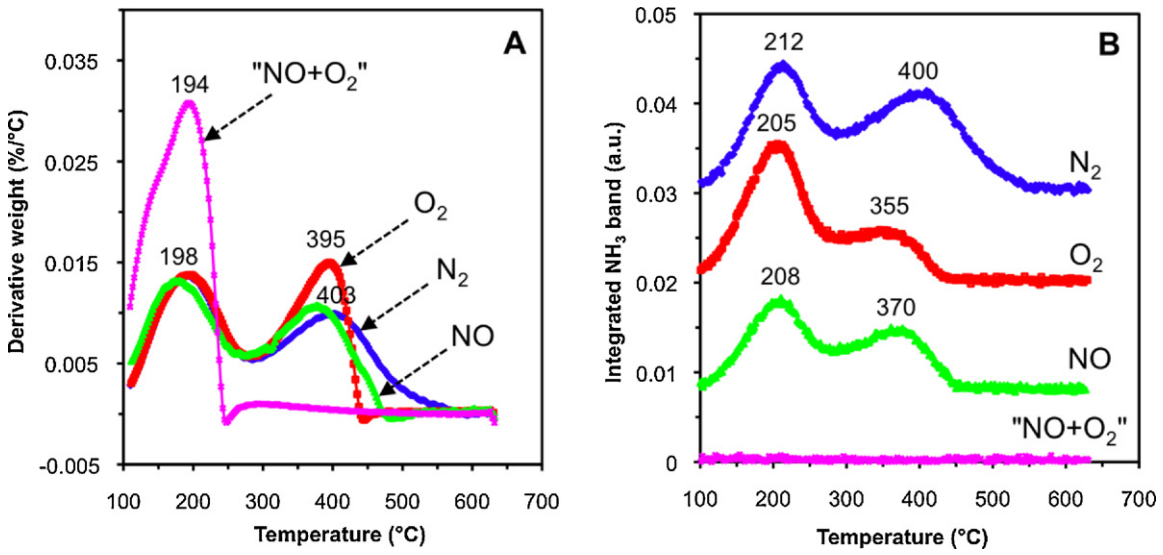

Fig. 4. DTG curves (A) and integrated NH_3 IR (B) during temperature-programmed release of NH_3(ad) on FeZ-1 in different environments (in NO, NO = 6000 ppm; in "NO + O_2", NO = 2000 ppm, O_2 = 16.8%).

act with NH_3(ad) on L acid sites while O_2 predominately interacts with NH_3(ad) on B acid sites. Addition of O_2 into the release system in NO environment accelerates the interaction, the majority of NH_3(ad) participated in the interactions. Therefore, the interaction routines of NH_3(ad) with NO and with "NO + O_2" over H-ZSM-5 were respectively proposed as follows:

In NO:

$$4NH_3(ad) + 6NO \rightarrow 5N_2 + 6H_2O \quad (2)$$

$$2NH_3(ad@Bacid) + 2NO \rightarrow 2N_2O + 3H_2 \quad (3)$$

In NO + O_2, NH_3(ad) on both acid sites could be removed by reactions (2) and (3). In addition, a fast interaction should exist:

$$2NH_3(ad) + NO + NO_2 \rightarrow 2N_2 + 3H_2O \quad (4)$$

The NO oxidation to NO_2 over H-ZSM-5 was confirmed in previous studies [41,42]. In fact, a moderate (<25%) NO_2 yield was observed in present work by a steady-state reaction of NO (500 ppm) and O_2 (4%). Sobalík et al. attributed the NO oxidation to NO_2 to the presence of impurities in the NH_4-ZSM-5 raw material [49].

3.3. Release of NH_3(ad) over Fe/H-ZSM-5

3.3.1. Effects of iron oxide and O_2 on the release of adsorbed NH_3

Fig. 4 shows the NH_3 release characteristics in different environments over sample FeZ-1. In the DTG curves (Fig. 4A), the peak temperatures of the NH_3(ad) release in N_2 over Fe/H-ZSM-5 were similar to those over H-ZSM-5: LT and HT peak temperatures appeared at 198 °C and 403 °C, respectively. This indicates that the deposition of iron oxide in H-ZSM-5 does not affect the strength of acidity. It is seen that both LT and HT peaks in O_2 and NO environments appeared at temperatures similar to those in N_2. But different weight-loss features were observed for the removal of NH_3(ad) from B acid sites: the ending temperature for complete removal of NH_3(ad) was 580 °C in N_2, 440 °C in O_2, and 480 °C in NO, respectively. These lower ending temperatures are attributable to the interaction between NH_3(ad) and O_2 or NO, which was also confirmed by the integrated IR bands during NH_3 release, as shown in Fig. 4B. It is obvious that the HT peak intensities of released NH_3 were decreased in both O_2 and NO environments. Also in NO environment, the LT peak intensity was significantly decreased. A more drastic change of DTG and released NH_3 IR curves occurred when the release of NH_3(ad) was performed in "NO + O_2" environment. Only one DTG peak at 194 °C was observed with the weight-loss ending temperature appeared at *ca* 240 °C. This peak is 88 °C lower than the HT peak of NH_3(ad) release over H-ZSM-5, where two DTG peaks at 135 °C and 282 °C existed. These drastic changes indicate that iron oxide contributes to the enhanced interaction.

To further investigate the effect of iron loading on the interaction between NH_3(ad) with reactive gases, a Fe/H-ZSM-5 sample (FeZ-2) was prepared with double the iron oxide loading. Fig. 5 shows DTG curves (Fig. 5A) and integrated NH_3 IR band (Fig. 5B) versus temperature. When the release was performed in a N_2 flow, the peak position over FeZ-2 was located at lower temperatures compared to FeZ-1. The IR band intensity of released NH_3 particularly from B acid sites was also lower than over sample FeZ-1. The difference could be attributable to the effect of increased coverage of iron oxide. The results are consistent with the change of NAC that decreased from 1.48 to 1.04, as listed in Table 1. When NH_3 release was carried out in O_2 or in NO, the NH_3 peaks over FeZ-2 were smaller than in N_2 (Fig. 5B), implying that part of the NH_3(ad) was removed by interaction. DTG curves (Fig. 5A) showed that the ending temperature for complete removal of NH_3(ad) appeared at 445 °C in O_2 and at 460 °C in NO, respectively, indicating that higher Fe loading still favors the interaction of NO with NH_3(ad) on B acid sites.

Over H-ZSM-5 (Figs. 2 and 3B) O_2 accelerates the interaction of NO with NH_3(ad) due to the participation of NO_2. The results in Fig. 4 have demonstrated that iron oxide can enhance such interaction in "NO + O_2" environment. Only a very small portion of NH_3(ad) was desorbed over H-ZSM-5 (Fig. 3B), but over FeZ-1 NH_3 desorption was no longer observed (Fig. 4B). Therefore, it would not have given any additional insight if the same high O_2 concentration (16.8%) were used to run the identical experiment over FeZ-2. To better see the role of O_2 concentration, we decided to use a much lower O_2 concentration (0.6% of O_2) to run the TPSI experiment over FeZ-2 in "NO + O_2" environment. The results of these experiments showed that for the TPSI of NH_3(ad) with NO_x, the O_2 concentration is very important. As seen in Fig. 5A, two peaks at 160 °C and 306 °C, instead of only one peak over FeZ-1, were observed for the removal of NH_3(ad) on L and B acid sites, respectively. Fig. 5B shows that NH_3(ad) on B acid sites could be removed

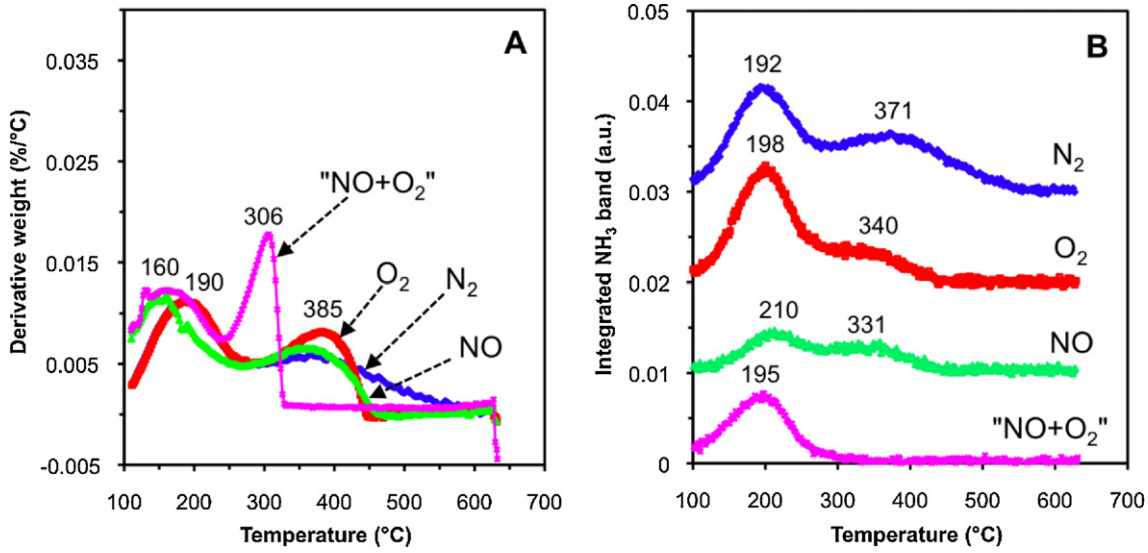

Fig. 5. DTG curves (A) and integrated NH_3 IR (B) during temperature-programmed release of NH_3(ad) on FeZ-2 in different environments (in NO, NO = 4000 ppm; in "NO + O_2", NO = 2000 ppm, O_2 = 0.6%).

by the interaction while the NH_3 peak at 195 °C was still there, indicating that a portion of the NH_3(ad) at L acid sites was released without participation in the interaction with NO_x. The ending temperature for complete removal of NH_3 was at 320 °C, 80 °C higher than that over FeZ-1. This experiment demonstrates that O_2 concentration may be a important factor for the removal of NH_3(ad) by the oxygen-involving NH_3(ad)–NO reaction.

Quantitative comparison of the amount of released NH_3 over Fe/H-ZSM-5 in different environments is shown in Table 3, represented by the percentage ratio of release in reactive environment to that in N_2. Consistent with the results over H-ZSM-5, the total released NH_3 amount over Fe/H-ZSM-5 followed the general order of "in N_2" > "in O_2" > "in NO" > "in NO + O_2". This order reflects the reactivity of NH_3(ad) with different reactive gases. As the NAC of FeZ-1 (1.43) is close to that of H-ZSM-5 (1.48), it should be reasonable to compare the role of iron oxide in FeZ-1 on the NH_3(ad) reactivity in O_2, NO and "NO + O_2" environments. In O_2, only 37% of NH_3(ad) on B acid sites of FeZ-1 was released compared to 71% of H-ZSM-5, indicating the enhancing role of iron oxide on the reactivity of NH_3(ad) on B acid sites with O_2. But there is no direct evidence that NH_3(ad) on L acid sites interacted with O_2 over Fe/ZSM-5, as the released NH_3 amount was 106% of that in N_2. Under the same environment, the released NH_3 amount over H-ZSM-5 was 82% of that in N_2, reflecting that 18% of NH_3(ad) was removed by the interaction with O_2. To account for this 106% result, NH_3 adsorption on iron oxide must be taken into consideration. Thus, additional NH_3 adsorption and desorption experiments were performed over iron oxide-supported on silica and MgO, respectively, which were prepared using the same impregnation method and calcination procedure. The results showed that the peak temperatures for NH_3 release over iron oxide supported on silica and MgO were located at the LT peak region of NH_3 release over Fe/H-ZSM-5. However, no such additional NH_3 adsorption effect was seen when NH_3(ad) was released in an NO environment, as NO prefers to interact with NH_3(ad) on L acid sites. Unlike the situation over H-ZSM-5 in NO environment, where higher percentages of NH_3 were released from B acid sites than from L acid sites, but over Fe/H-ZSM-5 smaller amounts of NH_3 were released from B acid sites than from L acid sites. This quantitatively confirms that iron oxide primarily enhances the interactions of NO with NH_3(ad) on B acid sites. In "NO + O_2" environment, the role of iron oxide is not so pronounced compared to H-ZSM-5 under the same conditions, due to NO_2 formation that accelerates the NH_3(ad)–NO_x interaction via fast SCR reaction. Nevertheless, the NH_3 amount released from L acid sites over Fe/H-ZSM-5 (4%) is still smaller than that (10%) over H-ZSM-5, as confirmed by the results shown in Figs. 2 and 4B.

The quantitative comparison of the effect of Fe loading on the released NH_3 amount is difficult, as some of the acid sites were physically covered by iron oxide in FeZ-2. Nevertheless, it still can be seen from Table 3 that NH_3(ad) on B acid sites is more readily removed by the interaction than NH_3(ad) on L acid sites. Only 8% of NH_3(ad) was released from B acid sites, compared to 62% from L acid sites.

3.3.2. *Release product of adsorbed NH_3 over Fe/H-ZSM-5*

To provide direct evidence for the interaction of NH_3(ad) with NO and NO_x over Fe/H-ZSM-5 samples, Figs. 6 and 7 show N-containing oxide products for the release in NO and in "NO + O_2", respectively. In NO (4000 ppm) environment, a wide negative NO

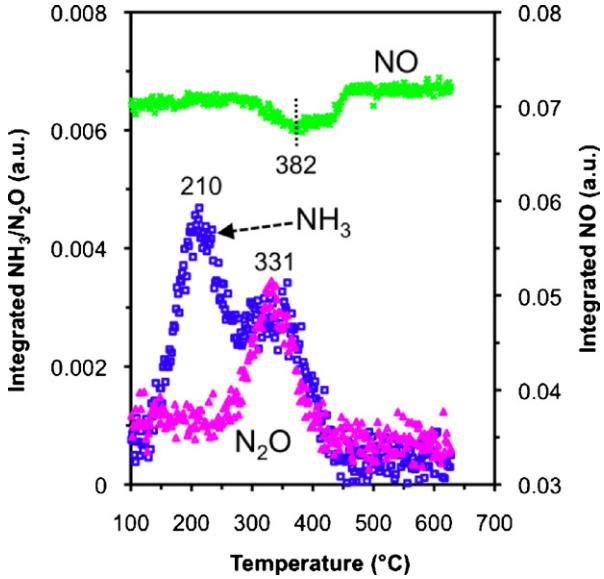

Fig. 6. Distribution of NH_3, N_2O, NO, and NO_2 during temperature-programmed release of NH_3(ad) on FeZ-2 in NO (4000 ppm) environment.

Table 3
Released NH_3 amount over Fe/ZSM-5 in different environments.

Released NH_3	FeZ-1			FeZ-2			
	In O_2	In NO[a]	In NO + O_2	In O_2	In NO[b]	In NO[c]	In NO + O_2[d]
Total (%)	68	56	4	59	51	38	28
L acid site (%)	106	70	4	98	65	38	62
B acid site (%)	37	45	3	35	44	38	8

[a] NO was 6000 ppm.
[b] NO was 2000 ppm.
[c] NO was 4000 ppm.
[d] O_2 was 0.6%.

peak was observed at 382 °C, corresponding to the NH_3 HT peak at 331 °C. This provides direct evidence for the enhancing role of iron oxide for the NO interaction with NH_3(ad) on B acid sites. An N_2O peak also appeared at the NH_3 HT peak temperature, similar to the results for NH_3 release over H-ZSM-5 (Fig. 3A), indicating that iron oxide in Fe/H-ZSM-5 is not exchanged with protons and does not change the interaction mechanism between NO and NH_3(ad), as Fe-exchanged species are active to catalyze N_2O decomposition [50,51]. In "NO + O_2" environment, all NH_3(ad) over Fe/H-ZSM-5 was removed by TPSI (Fig. 7A) while some of NH_3 (ad) on L acid sites was released over H-ZSM-5 (Fig. 3B). The negative peaks for simultaneous consumption of NO and NO_2 shifted to 204 °C, 82 °C lower than over H-ZSM-5. This temperature (204 °C) corresponds to the peak (194 °C) in DTG curves (Fig. 4A) for the removal of NH_3(ad) by TPSI with NO_x. This temperature (204 °C) is also located in the peak temperature region of the desorption of NH_3(ad) on L acid sites of H-ZSM-5 (Fig. 2B). These results indicate that iron oxide can enhance not only the interactions of NO_x with NH_3(ad) on B acid sites but also with NH_3(ad) on L acid sites. In addition, N_2O formation was not observed under this condition (Fig. 7A), indicating the modification role of O_2. When the oxygen concentration was decreased to 0.6% (Fig. 7B), the negative NO and NO_2 peaks shifted to 309 °C. This temperature is even 23 °C higher than that (286 °C) over H-ZSM-5 in 16.8% of O_2 and corresponds to the peak temperature (306 °C) in DTG curves (Fig. 5A) for removal of NH_3(ad) on B acid sites. Also, a strong NH_3 release peak appeared at 195 °C. These results confirm that the O_2 concentration plays a critical role in the fast interaction that proceeds preferentially with NH_3(ad) on B acid sites rather than on L acid sites. Iron oxide catalyzes both NO oxidation and fast interaction.

Sample characterizations by XRD, NH_3 adsorption, and N_2 physisorption showed that the Fe species in H-ZSM-5 are iron oxide. If exchanged Fe species existed in H-ZSM-5, the exchange into the proton positions of ZSM-5 would lead to the loss of Brønsted acid sites, and therefore, would result in a decrease of NH_3 adsorption capacity. Furthermore, these exchanged Fe species would catalyze N_2O conversion by decomposition [50], thereby eliminating N_2O effluent formation. TPSI experiments showed the formation of N_2O, which is attributable to the interaction of NO with NH_3(ad) on B acid sites. At least a couple of phenomena in the TPSI experiments confirmed the role of iron oxide in H-ZSM-5: (1) iron oxide enhances the NH_3(ad)–NO and NH_3(ad)–O_2 interactions, particularly for NH_3(ad) on B asid sites. The tentative interaction mechanism is likely through those iron oxide species located on pore edges of ZSM-5 channels, where the desorbing NH_3 species are additionally reacted with NO or O_2. (2) Iron oxide enhances the NH_3(ad)–(NO + O_2) interaction primarily via fast surface SCR where O_2 concentration plays a critical role.

It should be noted that a mechanical mixture sample composed of H-ZSM-5 and Fe_2O_3 could be easily made to distinguish the role of iron oxide. But with such Fe_2O_3–H-ZSM-5 mechanical mixtures it is difficult to achieve the high dispersion of iron oxide in H-ZSM-5. XRD characterization showed that in the present work the fast heating (80 °C/min) calcination led to the decomposition of $Fe(NO_3)_3$ on NH_4-ZSM-5 into highly dispersed iron oxide. TPSI experiments definitely provide a way to witness the interaction characteristics of adsorbed NH_3 with NO or NO_x, and can also provide insight into the effect of acid sites, the role of iron oxide, and the promotion of O_2, but they cannot present the dynamic reactivity of NH_3 under realistic reaction conditions, where too strong or too weak adsorption

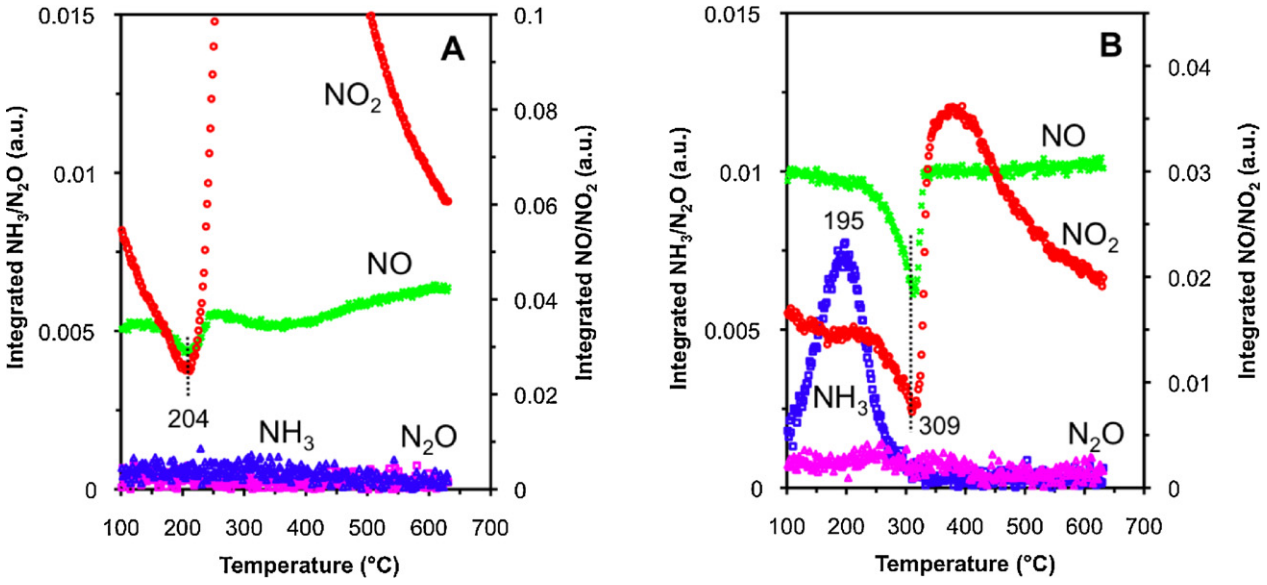

Fig. 7. Distribution of NH_3, N_2O, NO, and NO_2 during temperature-programmed release of NH_3(ad) on (A) FeZ-1 (O_2 = 16.8%) and (B) FeZ-2 (O_2 = 0.6%) in "NO + O_2" environment.

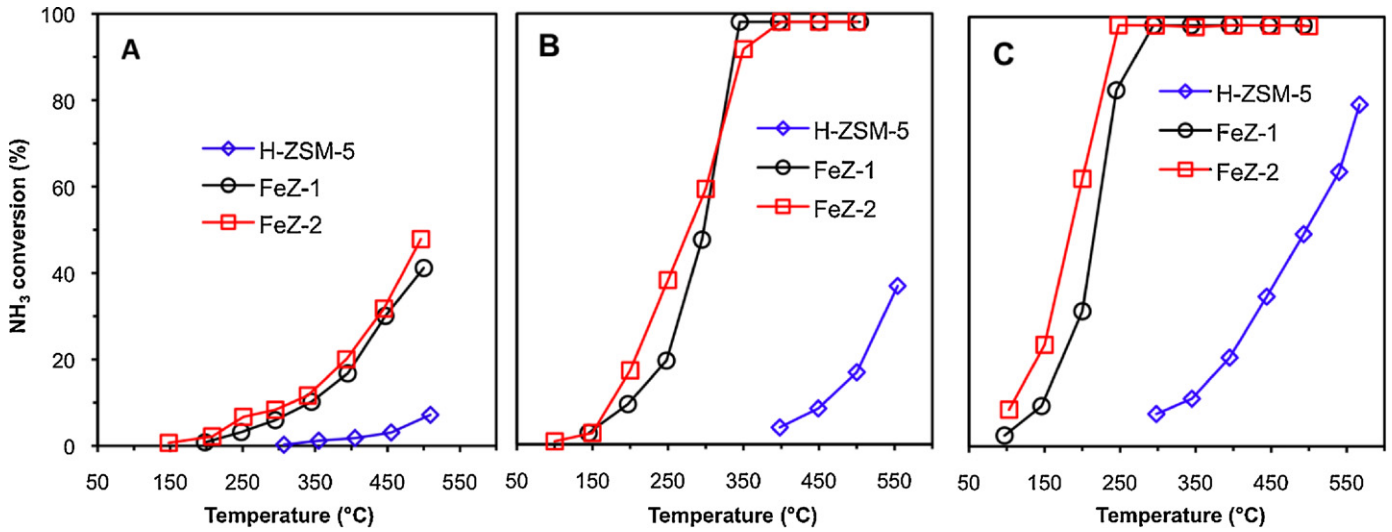

Fig. 8. NH_3 conversions in steady-state reaction systems of "$NH_3 + NO$" (A), "$NH_3 + O_2$" (B), and "$NH_3 + NO + O_2$" (C) over H-ZSM-5 and Fe/H-ZSM-5, respectively.

of NH_3 is unfavorable for NH_3 conversion. Therefore, the steady-state NH_3 reaction was evaluated over H-ZSM-5 and Fe/H-ZSM-5 in different reaction systems.

3.4. Steady-state reaction over H-ZSM-5 and Fe/H-ZSM-5

Fig. 8 shows the NH_3 conversion under different conditions. As expected, NH_3 can be converted over both Fe/H-ZSM-5 and H-ZSM-5. The presence of O_2 significantly promoted the NH_3 conversion leading to an order of the NH_3 reactivity with "$NH_3 + NO + O_2$" > "$NH_3 + O_2$" > "$NH_3 + NO$". This indicates that both acid sites and iron oxide are active to catalyze NH_3 reactions with O_2 and/or NO_x, confirming the results of TPSI experiments. It is also seen from Fig. 8 that the activity of Fe/H-ZSM-5 for all reactions of NH_3 with NO, O_2 and "$NO + O_2$" is much higher than the activity of H-ZSM-5. Consistent with TPSI results, a slightly higher NH_3 conversion was observed over FeZ-2 than over FeZ-1. With increasing reaction temperature, NH_3 conversions in all reaction systems increased. Complete NH_3 conversion was obtained at temperatures above 300 °C and 400 °C over Fe/H-ZSM-5 for the reaction systems of "$NH_3 + NO + O_2$" and "$NH_3 + O_2$", respectively. But over H-ZSM-5 the complete NH_3 conversion could not be achieved in the temperature range of the present work.

Fig. 8 also shows that the reactivity of NH_3 in the "$NH_3 + O_2$" reaction system is much higher than in "$NH_3 + NO$" over all samples. This is not surprising as iron oxide is a good catalyst for selective catalytic oxidation of NH_3 [52]. From the NH_3 release results (Table 2), the released NH_3 amount in NO was less than in O_2, implying that more adsorbed NH_3 participated in the reaction with NO than with O_2. It should be pointed out that N_2O formation was observed for "$NH_3 + NO$" and "$NH_3 + NO + O_2$" steady-state reactions over both H-ZSM-5 and Fe/H-ZSM-5. No noticeable N_2O formation was observed in "$NH_3 + O_2$". Products analysis by GC revealed N_2 formation for all steady-state reactions, particularly in the "$NH_3 + NO + O_2$" system. The observed N_2O formation supports the notion that the NH_3 activation mechanism could be not changed in the presence of iron oxide, as only exchanged Fe species are active for decomposition of N_2O [50,51].

In general, the insights gained from steady state experiments are consistent with the TPSI results. However, it is not surprising for there are some discrepancies between TPSI and steady-state reaction results, since the TPSI experiments were carried out in a TGA reactor where the fluid flow characteristics are quite different from a packed bed reactor.

3.5. Discussion

Both TPSI and the steady-state reactions indicate that NH_3 can be activated on acid sites for the reaction systems of "$NH_3 + NO$" and "$NH_3 + O_2$". The presence of O_2 in "$NH_3 + NO$" led to a significant increase of NH_3 conversion. Mechanistically, the participation of NO_2 in the SCR process is possible via the NO oxidation to NO_2, and the oxidation has been suggested as a rate-determining step over both H-ZSM-5 [39,42] and Fe/ZSM-5 [16,38,39,43] unless additional NO_2 is added into the reaction system until an NO_2/NO ratio of 1:1 is reached. It is well kown that the NO oxidation could be catalyzed by exchanged cationic Fe species [7,16,32,53] and is a pre-requistite and the rate-determining step for NH_3-SCR [16,43]. Recently iron oxide over ZSM-5 has also been recognized to be active for SCR of NO [14,22–24,54,55] and may accelerate the NO oxidation rate [27]. Once NO is oxidized, the formed NO_2 either participates in the fast SCR reaction [56] or directly desorbs into the gas effluent due to the configuration of the TGA reactor. Also, NO_2 is unlikely to adsorb on Fe-oxide particles [53,57]. This is why negative peaks for both NO and NO_2 were observed in the TPSI experiments (Figs. 3B and 7). Under steady-state reaction conditions, free NO_2 in the gas effluent would probably not exist as described in [15], as the desorbed NO_2 would take part in the fast SCR on adjacent sites down-stream in the packed-bed reactor. But a distinct NO oxidation (without addition of NH_3) to NO_2 effluent did occur over H-ZSM-5 in steady-state reactions, in agreement with [56] and with [41,42]. This case may be attributable to the impurities in H-ZSM-5 [49]. Over Fe/ZSM-5, free NO_2 is mentioned as a crucial intermediate in the mechanism proposed previously [32], where the role of iron is confined to NO oxidation and the subsequent fast SCR proceeds exclusively on B acid sites [36]. The TPSI experiments also showed that O_2 primarily interacts with NH_3(ad) on B acid sites, which was confirmed when 0.6% O_2 was added into the system, as shown in Table 3 and Fig. 7.

Iron oxide greatly enhances the NH_3(ad)–"$NO + O_2$" interaction, the main evidence being that there is only one DTG peak observed for the complete removal of adsorbed NH_3 at 194 °C (Fig. 4A). But, again when 0.6% O_2 was added into the TPSI system, the complete removal of NH_3(ad) by interaction on B acid sites shifted to 306 °C (Fig. 5A). The temperature for removal of NH_3(ad) on B acid sites in 0.6% O_2 over FeZ-2 is 24 °C higher than in 16.8% O_2 over H-ZSM-5. This provides clear evidence that O_2 promotes the interaction of NO_x with NH_3(ad) on both types of acid sites. While no NO_2 was added in the TPSI experiments, the simultaneous consumption peaks of NO and NO_2 even over H-ZSM-5 give direct evidence for

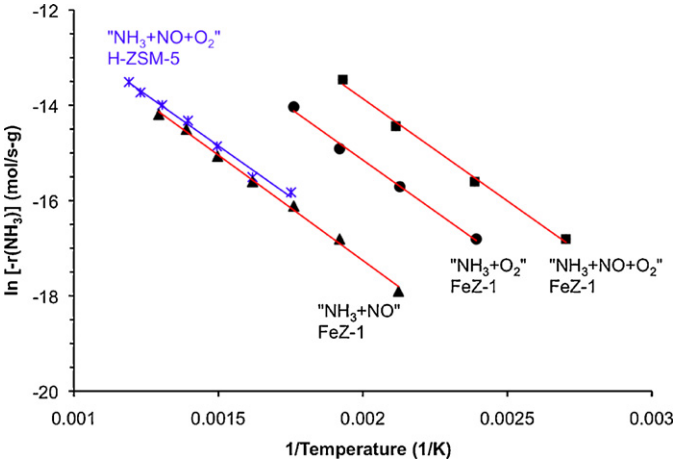

Fig. 9. Steady-state NH_3 conversion rate versus reciprocal temperature in different reaction systems over H-ZSM-5 and FeZ-1, respectively.

fast SCR. This strongly suggests that acid sites are active to catalyze NO to NO_2 oxidation.

NH_3 activation is a critical step for NH_3-SCR of NO [13,24,38]. According to the literature [15,32], the fast SCR takes place on the B acid sites but is strongly accelerated by exchanged Fe species. The question remains in the present work whether acid sites or iron oxide species are the predominant sites for ammonia activation. To elucidate the roles of iron oxide and acid sites, Fig. 9 compares the apparent activation energy that was estimated from NH_3 conversion in all three types of reactions over FeZ-1 and the reaction of "$NH_3 + NO + O_2$" over H-ZSM-5. Surprisingly, the activation energies for all the above-mentioned reactions are similar: 35.6 ± 3 kJ/mol. Iron oxide does not change the apparent activation energy barrier for NH_3 conversion. This result suggests that NH_3 adsorption and subsequent activation on acid sites in ZSM-5 is an essential step for NH_3 conversion. In NH_3 SCR of NO, it is unlikely that such a constant apparent activation energy for NO conversion would be observed, as additional NO_x could be generated from NH_3 oxidation [34].

Again for all TPSI experiments of adsorbed NH_3 with $NO + O_2$ over both H-ZSM-5 and Fe/H-ZSM-5, only one NO/NO_2 consumption peak was observed. This NO/NO_2 consumption peak temperature is related to the removal of NH_3(ad) on B acid sites, as confirmed by both weight-loss DTG and IR NH_3 curves (compare Fig. 2A with Fig. 3B, and Fig. 4A with Fig. 7A). This reveals that NH_3(ad) on the L acid sites may not be involved in the fast NH_3-SCR reaction or if so it participates in via a mechanism of NO oxidation to NO_2^- or NO_3^- [58]. Therefore, a dual mechanism over Fe/H-ZSM-5 may be exist over L and B acid sites in which iron oxide enhances both reactions. Specifically, iron oxide enhances NH_3 conversion over L acid sites in a process that excludes free NO_2 produced by NO oxidation [15,58], while iron oxide accelerates fast NH_3-SCR over B acid sites [36] where free NO_2 is consumed as an intermediate [56] as observed from TPSI experiments in "$NO + O_2$" environment.

4. Conclusions

NH_3 reactivity via NH_3 release in N_2, O_2, NO, and "$NO + O_2$" environments and dynamic steady-state reactions for NH_3 conversion by O_2, NO, and "$NO + O_2$" were investigated over H-ZSM-5 and iron oxide deposited H-ZSM-5 (Fe/H-ZSM-5). Fe/H-ZSM-5 was prepared by fast calcining $Fe(NH_3)_3/NH_4$-ZSM-5. The reactive gas had a quite different effect on NH_3 release performance. O_2 primarily interacted with NH_3(ad) on Brønsted acid sites while NO mainly interacted with NH_3(ad) on Lewis acid sites. The co-feeding of NO and O_2 significantly decreased the amount of released NH_3 compared to the individual NO or O_2 environment, due to the "fast" interaction of NO/NO_2 with NH_3(ad) at much lower temperatures. Iron oxide enhanced all interactions of adsorbed NH_3 with NO, O_2, and "$NO + O_2$", particularly for the interaction of NH_3(ad) on Brønsted acid sites. But iron oxide could not inhibit the N_2O formation for the NH_3(ad)–NO interaction, confirming that iron species are not exchanged with protons of H-ZSM-5. A pronounced O_2 promotion on NO_x interaction with NH_3(ad) on both acid sites was observed by TPSI. As no additional NO_2 was fed in the "$NO + O_2$" reaction system, the formation of NO_2 is attributable to NO oxidation that was accelerated by iron and promoted by O_2 concentration.

Both O_2 promotion and the catalyzing role of iron oxide were confirmed by steady-state reactions of "$NH_3 + NO$", "$NH_3 + O_2$", and "$NH_3 + NO + O_2$", where the NH_3 conversion followed the order of "$NH_3 + NO$" < "$NH_3 + O_2$" < "$NH_3 + NO + O_2$". But iron oxide did not decrease the apparent activation energy barrier for NH_3 conversion. Based on the results of TPSI and steady-state reactions, it appears that both acid sites and iron oxide are essential for accelerating the NH_3-SCR of NO in excess of O_2, where Lewis and Brønsted acid sites may play dual role for the activation of NH_3(ad) and conversion via fast reactions with NO_x.

Acknowledgements

Support of this work by General Motors Global Research and Development is gratefully acknowledged. The authors thank Dr. Hui Feng for sample characterization by NH_3 adsorption. Helpful discussions with Dr. Galen Fisher are gratefully acknowledged.

Appendix A. Supplementary data

Supplementary data associated with this article can be found, in the online version, at doi:10.1016/j.cattod.2011.05.010.

References

[1] T.V. Johnson, SAE technical paper 2010-01-0301 (2010).
[2] X. Chen, J. Schwank, Top. Catal. 46 (2007) 39.
[3] A. Lindholm, H. Sjövall, L. Olsson, Appl. Catal. B 98 (2010) 112.
[4] J.R. Theis, J.A. Ura, R.W. McCabe, SAE technical paper 2010-01-0300 (2010).
[5] H.-Y. Chen, E.C. Weigert, J.M. Fedeyko, J.P. Cox, P.J. Andersen, SAE technical paper 2010-01-0302 (2010).
[6] D. Chatterjee, P. Koci, Volker Schmeisser, M. Marek, M. Weibel, SAE technical paper 2010-01-0887 (2010).
[7] S. Brandenberger, O. Kröcher, A. Tissler, R. Althodff, Catal. Rev. 50 (2008) 492.
[8] M. Schwidder, M.S. Kumar, K. Klementiew, M.M. Pohl, A. Brückner, W. Grünert, J. Catal. 231 (2005) 314.
[9] H.-Y. Chen, W.M.H. Sachtler, Catal. Today 42 (1998) 73.
[10] G. Qi, R.T. Yang, Appl. Catal. B 60 (2005) 13.
[11] P. Marturano, L. Drozdova, A. Kogelbauer, R. Prins, J. Catal. 192 (2000) 236.
[12] M. Iwasaki, K. Yamazaki, K. Banno, H. Shinjoh, J. Catal. 260 (2008) 205.
[13] S. Brandenberger, O. Kröcher, A. Wokaun, A. Tissler, R. Althoff, J. Catal. 268 (2009) 297.
[14] M.S. Kumar, M. Schwidder, W. Grünert, U. Bentrup, A. Brückner, J. Catal. 239 (2006) 173.
[15] M. Schwidder, S. Heikens, A.D. Toni, S. Geisler, M. Berndt, A. Brückner, W. Grünert, J. Catal. 259 (2008) 96.
[16] M. Devadas, O. Kröcher, M. Elsener, A. Wokaun, G. Mitrikas, N. Söger, M. Pfeifer, Y. Demel, L. Mussmann, Catal. Today 119 (2007) 137.
[17] N. Apostolescu, B. Geiger, K. Hizbullah, M.T. Jan, S. Kureti, D. Reichert, F. Schotta, W. Weisweiler, Appl. Catal. B 62 (2006) 104.
[18] L. Chmielarz, P. Kustrowski, M. Zbroja, W. Lasocha, R. Dziembaj, Catal. Today 90 (2004) 43.
[19] G.-H. Yao, F. Wang, X.-B. Wang, K.-T. Gu, Energy 35 (2010) 2295.
[20] H. Bosch, F. Janssen, Catal. Today 2 (1988) 369.
[21] G. Ramis, L. Yi, M. Turco, E. Kotur, R.J. Willey, J. Catal. 157 (1995) 523.
[22] M. Schwider, F. Heinrich, M.S. Kumar, A. Bruckner, W. Grünert, Stud. Surf. Sci. Catal. 154 (2004) 2484.
[23] Q. Zhu, R.M. van Teeffelen, R.A. van Santen, E.J.M. Hensen, J. Catal. 221 (2004) 575.
[24] Z. Liu, P.J. Millington, J.E. Bailie, R.R. Rajaram, J.A. Anderson, Micropor. Mesopor. Mater. 104 (2007) 159.
[25] P. Balle, B. Geiger, S. Kureti, Appl. Catal. B 85 (2009) 109.

[26] M. Høj, M.J. Beier, J.-D. Grunwaldt, S. Dahl, Appl. Catal. B 93 (2009) 166.
[27] R. Serra, M.J. Vecchietti, E. Miró, A. Boix, Catal. Today 133–135 (2008) 480.
[28] D. Klukowski, P. Balle, B. Geiger, S. Wagloehner, S. Kureti, B. Kimmerle, A. Baiker, J.-D. Grunwaldt, Appl. Catal. B 93 (2009) 185.
[29] M. Schwidder, M.S. Kumar, U. Bentrup, J. Perez-Ramirez, A. Brückner, W. Grünert, Micropor. Mesopor. Mater. 111 (2008) 124.
[30] N.Y. Topsoe, H. Topsoe, J.A. Dumesic, J. Catal. 151 (1995) 226.
[31] M.D. Amiridis, R.V. Duevel, I.E. Wachs, Appl. Catal. B 20 (1999) 111.
[32] R.Q. Long, R.T. Yang, J. Catal. 207 (2002) 224.
[33] D.A. Peña, B.S. Uphade, P.G. Smirniotis, J. Catal. 221 (2004) 421.
[34] A.C. Akah, G. Nkeng, A.A. Garforth, Appl. Catal. B 74 (2007) 34.
[35] A. Kato, S. Matsuda, F. Nakajima, H. Huroda, T. Narita, J. Phys. Chem. 85 (1981) 4099.
[36] M. Devadas, O. Kröcher, M. Elsener, A. Wokaun, N. Söger, M. Pfeifer, Y. Demel, L. Mussmann, Appl. Catal. B 67 (2006) 187.
[37] M. Koebel, M. Elsener, G. Madia, SAE Technical Paper 2001-01-3625 (2001).
[38] M. Iwasaki, K. Yamazaki, H. Shinjoh, Appl. Catal. A: Gen. 366 (2009) 84.
[39] K. Rahkamaa-Tolonen, T. Maunula, M. Lomma, M. Huuhtanen, R.L. Keiski, Catal. Today 100 (2005) 217.
[40] Q. Sun, Z.X. Gao, H.-Y. Chen, W.M.H. Sachtler, J. Catal. 201 (2001) 89.
[41] R. Matarrese, H.H. Ingelsten, M. Skoglundh, J. Catal. 258 (2008) 386.
[42] M. Wallina, C.-J. Karlssona, A. Palmqvista, M. Skoglundh, Top. Catal. 30/31 (2004) 107.
[43] H.Y. Huang, R.Q. Long, R.T. Yang, Appl. Catal. A: Gen. 235 (2002) 241.
[44] B.M. Lok, B.K. Marcus, C.L. Angell, Zeolites 6 (1986) 185.
[45] S.G. Hegde, R. Kumar, R.N. Bhat, P. Ratnasamy, Zeolites 9 (1989) 231.
[46] A.L. Kustov, T.W. Hansen, M. Kustova, C.H. Christensen, Appl. Catal. B 76 (2007) 311.
[47] N. Katada, H. Igi, J. Kim, M. Niwa, J. Phys. Chem. B 101 (1997) 5969.
[48] X. Chen, J. Schwank, J. Li, W.F. Schneider, C.T. Goralski Jr., P.J. Schmitz, Appl. Catal. B 61 (2005) 189.
[49] Z. Sobalík, P. Kubánek, O. Bortnovsky, A. Vondrová, Z. Tvarůková, J.E. Šponer, B. Wichterlová, Stud. Surf. Sci. Catal. 142 (2002) 533.
[50] I. Melián-Cabrera, F. Kapteijn, J.A. Moulijn, Catal. Today 110 (2005) 255.
[51] K. Sun, H. Xia, E. Hensen, R. van Santen, C. Li, J. Catal. 238 (2006) 186.
[52] H.M.J. Kušar, A.G. Ersson, M. Vosecký, S.G. Järås, Appl. Catal. B 58 (2005) 25.
[53] G. Delahay, D. Valade, A. Guzmán-Vargas, B. Coq, Appl. Catal. B 55 (2005) 149.
[54] M.S. Kumar, M. Schwidder, W. Grünert, A. Brückner, J. Catal. 227 (2004) 384.
[55] M. Schwidder, F. Heinrich, M.S. Kumar, A. Brückner, W. Grünert, Stud. Surf. Sci. Catal. 154 (2004) 2484.
[56] O. Kröcher, M. Devadas, M. Elsener, A. Wokaun, N. Söger, M. Pfeifer, Y. Demel, L. Mussmann, App. Catal. B 66 (2006) 208.
[57] A. Sierraalta, P.K. Roy, M.R. Brussin, J. Catal. 205 (2002) 107.
[58] P. Forzatti, L. Lietti, I. Nova, E. Tronconi, Catal. Today 151 (2010) 202.